

# Low-Temperature Phase of the $\text{Cd}_2\text{Re}_2\text{O}_7$ Superconductor: *Ab initio* Phonon Calculations and Raman Scattering

Konrad J. Kapcia,<sup>1,\*</sup> Maureen Reedyk,<sup>2</sup> Mojtaba Hajialamdari,<sup>2</sup> Andrzej Ptok,<sup>1</sup>  
Przemysław Piekarczyk,<sup>1</sup> Fereidoon S. Razavi,<sup>2</sup> Andrzej M. Oleś,<sup>3,4</sup> and Reinhard K. Kremer<sup>4</sup>

<sup>1</sup>*Institute of Nuclear Physics, Polish Academy of Sciences, ul. W. E. Radzikowskiego 152, PL-31342 Kraków, Poland*

<sup>2</sup>*Department of Physics, Brock University, St. Catharines, ON, L2S 3A1, Canada*

<sup>3</sup>*Marian Smoluchowski Institute of Physics, Jagiellonian University, Prof. S. Łojasiewicza 11, PL-30348 Kraków, Poland*

<sup>4</sup>*Max Planck Institute for Solid State Research, Heisenbergstrasse 1, D-70569 Stuttgart, Germany*

(Dated: June 25, 2019)

Using an *ab initio* approach, we report a phonon soft mode in the tetragonal structure described by the space group  $I4_122$  of the 1 K  $5d$  superconductor  $\text{Cd}_2\text{Re}_2\text{O}_7$ . It induces an orthorhombic distortion to a crystal structure described by the space group  $F222$  which hosts the superconducting state. This new phase has a lower total energy than the other known crystal structures of  $\text{Cd}_2\text{Re}_2\text{O}_7$ . Comprehensive temperature dependent Raman scattering experiments on isotope enriched samples,  $^{116}\text{Cd}_2\text{Re}_2^{18}\text{O}_7$ , not only confirm the already known structural phase transitions but also allow us to identify a new characteristic temperature regime around  $\sim 80$  K, below which the Raman spectra undergo remarkable changes with the development of several sharp modes and mode splitting. Together with the results of the *ab initio* phonon calculations we take these observations as strong evidence for another phase transition to a novel low-temperature crystal structure of  $\text{Cd}_2\text{Re}_2\text{O}_7$ .

Superconductivity in materials with non-centrosymmetric crystal structures currently attracts broad attention [1, 2]. When parity is not a good quantum number anymore, antisymmetric spin-orbit coupling may mix spin-singlet with spin-triplet components within the superconducting (SC) state [3]. Materials containing heavy  $4d$  ( $5d$ ) transition metal elements with large spin-orbit coupling are especially promising candidates to search for such states [4]. Strong spin-orbit coupling in correlated electron system can realize unconventional quantum ground state, as pointed out recently [5, 6].

The ternary oxide  $\text{Cd}_2\text{Re}_2\text{O}_7$  (CRO) containing the  $5d$  transition metal Re is the first discovered pyrochlore oxide superconductor with  $T_c \simeq 1$  K [7–9]. Among a number of unusual properties reported for CRO, a series of structural phase transitions (SPTs) is of particular interest since they essentially determine the low-temperature (LT) structural and electronic properties [10]. In order to understand the character of the SC state it proved of especial importance to characterize the crystal structure at lowest temperatures. At room temperature (RT) CRO crystallizes in a cubic structure (phase I,  $Fd\bar{3}m$ , no. 227). The 1<sup>st</sup> SPT to a non-centrosymmetric tetragonal structure (phase II,  $I\bar{4}m2$ , no. 119) takes place at  $\sim 200$  K and a subsequent first order SPT at  $\sim 120$  K to another non-centrosymmetric tetragonal structure (phase III,  $I4_122$ , no. 98) [11, 12], see Fig. 1. So far, it is a common belief that this latter phase is the crystal structure in which superconductivity in CRO occurs.

Both currently known LT tetragonal space groups (phase II and phase III) are subgroups of the RT cubic space group, see Fig. 1. The structural order parameter transforms according to the irreducible representation  $E_u$  [13, 14]. The purpose of this Letter is to highlight the discovery of a novel non-centrosymmetric orthorhombic LT

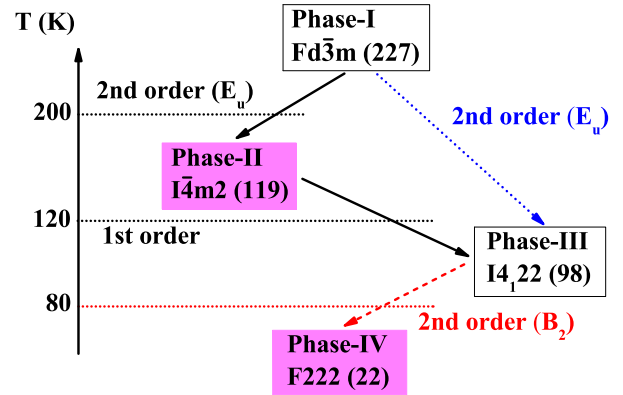


FIG. 1. Different phases of  $\text{Cd}_2\text{Re}_2\text{O}_7$  (see text). Solid lines denote the SPTs observed experimentally. For the second-order SPTs, the irreducible representations of the associated soft modes are indicated. Magenta boxes denote dynamically stable phases in our *ab initio* phonon studies.

phase (phase IV, space group  $F222$ , no. 22) for which we find strong evidence both from density functional theory (DFT) calculations of the phonon dispersions and detailed temperature dependent Raman scattering experiments on isotopically enriched single crystals.

Whereas the SPT at  $\sim 200$  K leads to pronounced anomalies, e.g. in the specific heat, the electrical resistivity, the Pauli susceptibility, or the thermal expansion, the SPT at  $\sim 120$  K is barely perceivable in the bulk properties [15, 16]. A hysteresis in the electrical resistivity points to a 1<sup>st</sup> order SPT [10, 15]. The impact of the SPT on the electronic band structure of CRO has been studied within DFT [17–19]. A semimetallic band structure with heavy bands near  $E_F$ , heavy hole bands near the zone boundary, and relatively light electron pockets

around the  $\Gamma$  point were found. The states near  $E_F$  are sensitive to spin-orbit coupling whereas on-site Coulomb interaction  $U$  has negligible effect on Re  $5d$  states which are predominantly itinerant. The SPTs markedly change the carrier density near  $E_F$ , as observed in an inversion of the Hall coefficient and rapid decrease of the spin susceptibility below  $\sim 200$  K [19, 20]. In view of the low carrier density and the heavy band masses, an excitonic instability of the Fermi surface was suggested as the origin of the I  $\rightarrow$  II SPT [18].

The structural distortions induced by the SPTs of CRO are particularly very minute and difficult to detect by x-ray or neutron scattering techniques [10]. Raman scattering experiments played therefore a central role to ascertain the SPTs in CRO, and were also employed to elucidate the lattice dynamical properties and the role of electron-phonon coupling [21–25]. Below the SPT at  $\sim 200$  K, Kendziora *et al.* [21] observed a peak at zero frequency in the Raman spectra with divergent intensity which they ascribed to a Goldstone-mode type excitation that develops due to the breaking of the continuous symmetry at the SPT. This interpretation has been questioned by Harter *et al.* [26] who argued that the apparent decrease in the Raman center frequency as the temperature of the SPT is approached from below, could be due to a reduction of the phonon lifetime, a conclusion supported by the time-resolved optical reflectivity. It was proposed that multipolar nematic order rather than a structural distortion drives the inversion symmetry breaking [27].

Clearly there is a need for further investigation, but regardless of softening and hardening of phonons and the appearance of new Raman modes below 200 K and 120 K supports symmetry reduction due to SPTs. The Raman spectra indicated the structural changes at 200 K and 120 K to occur in the Re–O(1) network, with O(1) being the oxygen atoms at the apices of the  $\text{ReO}_6$  octahedra [23]. Phonon spectra have also been studied by IR and ultrafast coherent phonon spectroscopy [26, 28, 29]. Optical conductivity studies revealed that the LT CRO is quite different from a simple metal [28] and exhibits anomalous Fermi liquid behavior at LT [30]. Evidence for strong electron-phonon coupling and enhanced quasi-particle damping possibly related to a SPT within the SC region was also found from an analysis of the temperature dependence of the optical conductivity [29], and from Andreev reflection spectroscopy [31].

Our DFT calculations were performed using the projector augmented-wave method [32, 33], within the generalized gradient approximation (GGA) [34], implemented in the VASP program package [35]. A  $\mathbf{k}$ -mesh of  $4 \times 4 \times 4$  points in the Monkhorst-Pack scheme was used for integration in the reciprocal space and an energy cut-off for the plane wave expansion of 500 eV was applied. The lattice constants as well as the atom positions were optimized within the supercells of 88 atoms, employing the

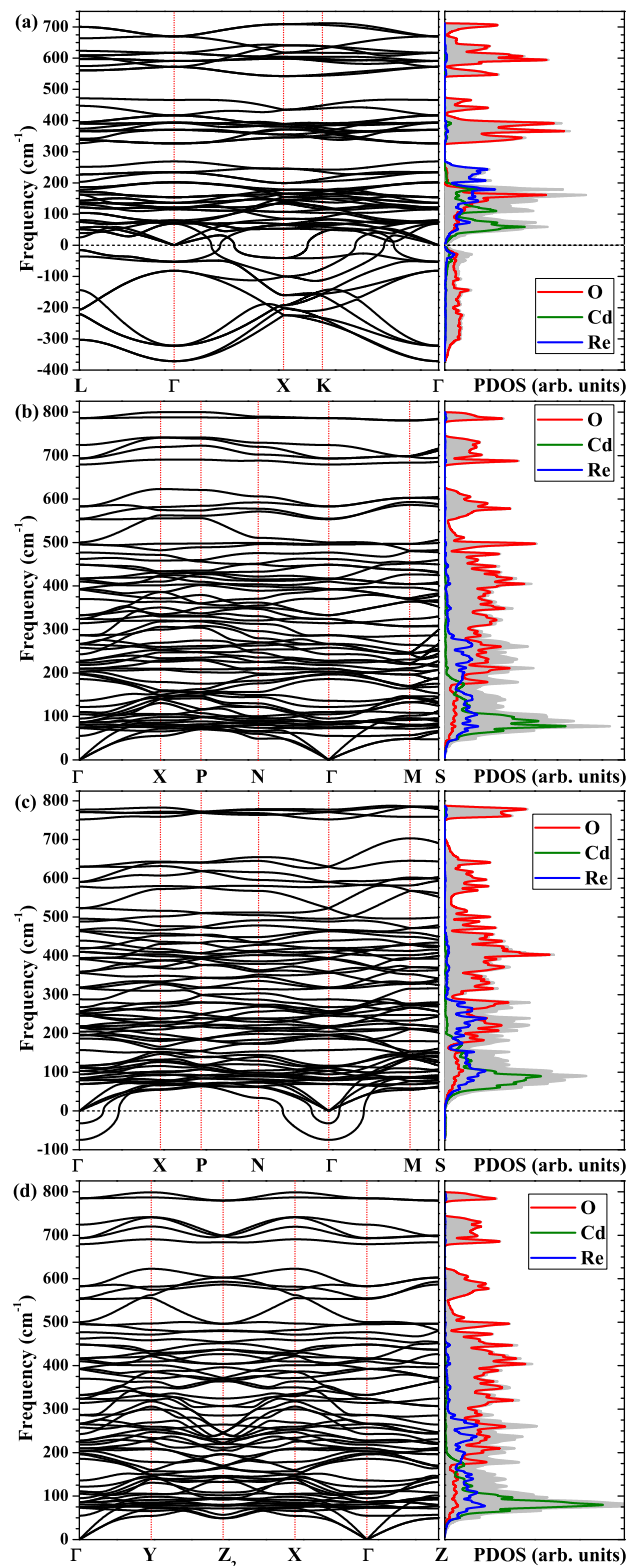


FIG. 2. The phonon dispersion curves (left) and partial PDOSs (right) for each phase: (a)  $Fd\bar{3}m$  phase I, (b)  $I4m2$  phase II, (c)  $I4_122$  phase III, and (d)  $F222$  phase IV. The gray shaded areas represent the total PDOS.

conjugate gradient technique and energy convergence criteria of  $10^{-8}$  ( $10^{-6}$ ) eV for electronic (ionic) iterations.

The phonon dispersions and phonon density of states (PDOS) for the possible structures of CRO were calculated using the direct method [36] implemented in the PHONON software [37], see Fig. 2. Since the number of atoms in the primitive cells of all structures is 22, all phases have 66 phonon modes. The phonon spectra in phase I and phase III exhibit imaginary (soft) modes indicating that these phases are dynamically unstable at  $T = 0$ . The most unstable is the cubic structure (phase I) with imaginary modes found for each wave vector. The lowest soft phonon is a doubly degenerate mode with the irreducible representation  $E_u$  which agrees with the group theory analysis [13] and the previous DFT study [14]. This indicates the displacive character of the I  $\rightarrow$  II SPT connected with the soft mode, although one cannot rule out a more complex mechanism involving electron-phonon interactions. Regardless of the mechanism of the SPT, our calculations show that the total energy of the tetragonal phase II is lowered by  $-2.085$  eV and it is dynamically stable with all phonon branches being real.

Surprisingly, in the tetragonal phase III we found the soft modes close to the  $\Gamma$  point. The irreducible representation of the lowest imaginary mode is here  $B_2$ . Group theory analysis shows that this mode breaks tetragonal symmetry and generates the orthorhombic non-centrosymmetric structure (space group  $F222$ ), called phase IV. We obtained its crystal structure using the polarization vectors of the  $B_2$  soft mode and optimized its crystal structure parameters, see the Appendix. The orthorhombic distortion is very weak with the difference between the  $a$  and  $b$  lattice parameters about 0.004%. The total energy of this structure is lower than that of the tetragonal phase III by only  $-0.06$  eV and it is very close to phase II ( $-0.00005$  eV). Even though these differences are very small, modern implementations of the DFT method assure reliability of such results [38]. To confirm the dynamical stability of phase IV, we also calculated phonon dispersions and found only stable (real) modes, see Fig. 2(d).

The contribution of particular atoms to the phonon spectra can be analyzed using the PDOS, see Fig. 2. Vibrations of the heavy Cd atoms prevail below  $100$   $\text{cm}^{-1}$ , while Re atoms vibrate mainly with frequencies  $\omega \in (0, 300)$   $\text{cm}^{-1}$ . Above  $300$   $\text{cm}^{-1}$ , the spectra are dominated by oxygen vibrations with the cut-off around  $700$  ( $800$ )  $\text{cm}^{-1}$  in the cubic (tetragonal) structures. The soft modes found in the cubic phase largely contribute to the PDOS, with the dominant component of oxygen vibrations. In contrast, the soft modes have negligible weight in the total PDOS in the  $I4_122$  tetragonal phase.

Oxygen and cadmium isotope-substituted single crystals of CRO have been prepared by chemical vapor transport [24]. All handling of the charges was carried out in a water and oxygen free glove box, ensuring almost com-

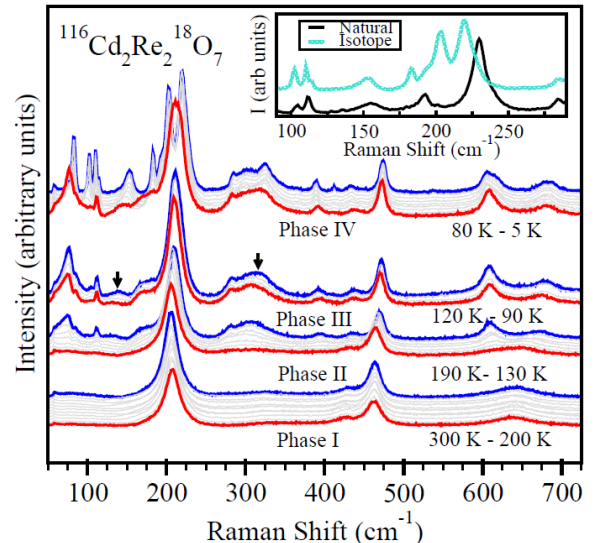


FIG. 3. Raman spectra of  $^{116}\text{Cd}_2\text{Re}_2^{18}\text{O}_7$  in four characteristic temperature regimes (shifted along the  $y$ -axis for clarity). In each regime the red/lower (blue/upper) curve is at the highest (lowest) temperature, and the gray curves show the evolution in steps of 10 K. The arrows mark regions where subtle changes are found in phase III. The upper inset displays a comparison of two Raman spectra collected in Phase IV at 25 K of a crystal with the natural oxygen isotope (99.8%  $^{16}\text{O}$ ) abundance, and of a crystal of  $^{116}\text{Cd}_2\text{Re}_2^{18}\text{O}_7$  at 20 K.

plete  $^{18}\text{O}$  substitution in the final product. This was confirmed by measuring the shift in the frequency of oxygen phonon modes [24]. Heat capacity measurements on such crystals showed a clear  $\lambda$ -type anomaly at the SPT from phase I to phase II at  $\sim 204$  K and a very faint anomaly at  $\sim 114$  K indicating the SPT from phase II to phase III, in good agreement with earlier reports [10]. The superconducting transition at  $T_c \sim 1$  K in crystals of  $^{116}\text{Cd}_2\text{Re}_2^{18}\text{O}_7$  is also seen in the heat capacity and ac-susceptibility data (see Figs. 1 and 2 in the Appendix). Polarized Stokes Raman scattering measurements were performed in a back-scattering geometry using the 632.8 nm line of a Helium-Neon laser at  $T \in (5, 300)$  K. The measurements were carried out on the natural growth plane (111) with parallel scattering geometry. The Raman scattering cross-section contains an  $\omega^4$  factor due to Rayleigh scattering which gives a monotonically decreasing contribution to the background. Its temperature dependence is subject to the Bose-Einstein factor for thermally excited oscillators. Therefore, we multiplied our spectra by

$$\frac{1}{[n(\omega_\sigma) + 1]\omega_s^4} = \frac{1}{[n(\omega_\sigma) + 1](\omega_o - \omega_\sigma)^4}, \quad (1)$$

where  $\omega_o$  is the laser frequency,  $\omega_\sigma$  is the Raman shift,  $\omega_s$  is the absolute frequency of the scattered light, and

$n(\omega_\sigma) = 1/[\exp(\hbar\omega_\sigma/k_B T) - 1]$  is the Bose-Einstein factor for thermally excited oscillators.

The Raman spectra of  $^{116}\text{Cd}_2\text{Re}_2^{18}\text{O}_7$  are displayed for four characteristic temperature regimes in Fig. 3. From 300 K to 200 K, i.e., in the cubic  $Fd\bar{3}m$  phase I, the spectra exhibit five of the six Raman active oxygen modes expected from a factor group analysis in agreement with previous experiments [23, 24]. The modes near  $425\text{ cm}^{-1}$  and  $650\text{ cm}^{-1}$  have been assigned to  $T_{2g}$  modes and the mode near  $460\text{ cm}^{-1}$  to the  $A_{1g}$  mode. The mode near  $200\text{ cm}^{-1}$  is comprised of overlapping  $E_g$  and  $T_{2g}$  modes [25]. The absent  $T_{2g}$  mode is likely too weak to be resolved, consistent with previous studies [22–24]. In addition, there is a broad feature near  $350\text{ cm}^{-1}$ , which evolves into a broad mode situated near  $300\text{ cm}^{-1}$  when the temperature is lowered below 200 K.

The transition to the tetragonal  $I\bar{4}m2$  phase below 200 K results in other significant changes to the phonon spectrum including a splitting of the mode near  $640\text{ cm}^{-1}$ , and additional modes appearing below  $175\text{ cm}^{-1}$ . This is consistent with the prediction of a number of additional Raman active modes according to the factor group analysis. We observed only very subtle changes at the temperature of the second SPT from tetragonal  $I\bar{4}m2$  to  $I4_122$  (II  $\rightarrow$  III) near 115 K as shown by the arrows in Fig. 3.

Here we focus on the low frequency Raman scattering in the novel phase IV. As the temperature is lowered from 80 K there are further prominent changes at Raman shifts lower than  $250\text{ cm}^{-1}$  (see Fig. 4). Figure 4(a) shows that the spectrum begins to evolve rapidly near  $\sim 80\text{ K}$  from that characteristic for phase III (the 90 K curve), while Fig. 4(b) shows that several sharp peaks develop upon further lowering of the temperature.

Further evidence for  $T \simeq 80\text{ K}$  being a characteristic temperature for a SPT from phase III to phase IV, comes from the behavior of the  $E$  mode near  $210\text{ cm}^{-1}$  in Fig. 5. This mode is derived from oxygen motion as shown by the shift with  $^{16}\text{O}$  isotopic substitution by  $^{18}\text{O}$  (upper inset in Fig. 5). At temperatures above the cubic to tetragonal SPT at 200 K, one observes a slight softening of the center frequency of the mode with decreasing temperature. Below the SPT at 200 K the mode begins to harden as the temperature is lowered, followed by a remarkable splitting with an onset near 80 K which reaches  $\sim 18\text{ cm}^{-1}$  at the lowest temperatures, highlighted in the lower inset in Fig. 5. As obtained by group theory, the doubly degenerate Raman mode  $E$  in the  $I4_122$  structure splits into two modes ( $B_2$  and  $B_3$ ) in the  $F222$  structure. Whereas the lower branch fits nicely to a critical power law indicating a continuous SPT as predicted by the DFT results, the transition to the upper branch is steeper (see the Appendix for more details). A full splitting of the  $210\text{ cm}^{-1}$  mode has not been reported before. However, Bae *et al.* [23] and Knee *et al.* [22] saw a shoulder and weak modes at the low-energy side of the  $210\text{ cm}^{-1}$  mode. We

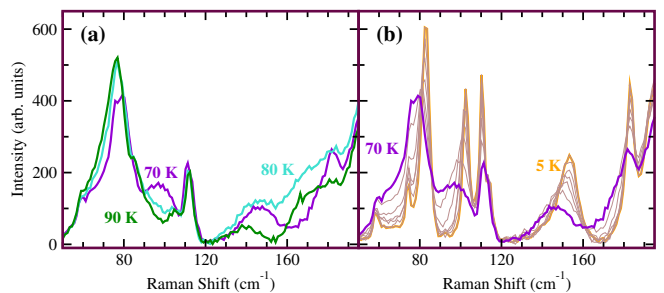


FIG. 4. Low frequency Raman scattering spectrum of  $^{116}\text{Cd}_2\text{Re}_2^{18}\text{O}_7$  showing: (a) the SPT III  $\rightarrow$  IV and (b) the temperature evolution within phase IV.

consider the distinct splitting of the  $210\text{ cm}^{-1}$  mode as strong support for an additional LT SPT consistent with our conclusions from the DFT calculations. The symmetry reduction of the SPT, III  $\rightarrow$  IV, leads to eight different oxygen sites in a unit cell slightly larger than that of the cubic structure, see Table I in the Appendix.

It remains puzzling why, so far, we could observe clear evidence for the SPT from phase III to phase IV only in oxygen isotope substituted samples, possibly indicating that the SPT at  $\sim 80\text{ K}$  can only be induced or stabilized by increasing the mass of the oxygen atoms. A similar observation has been made for  $\text{SrTiO}_3$  where in crystal containing only  $^{16}\text{O}$  the transition to a ferroelectric

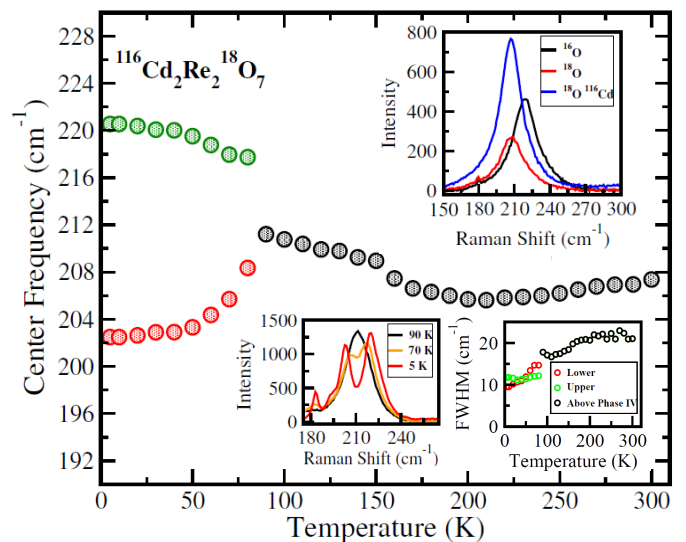


FIG. 5. Temperature variation of the center frequency of the  $210\text{ cm}^{-1}$  mode for  $^{116}\text{Cd}_2\text{Re}_2^{18}\text{O}_7$ . Note the splitting at  $\sim 80\text{ K}$ . The lower insets show the mode at temperatures just above/below 80 K and at 5 K and the full-width-half maximum of the mode above and below the structural phase transition. The upper inset displays this mode measured for a crystal with the natural oxygen isotope (99.8%  $^{16}\text{O}$ ), for an  $^{18}\text{O}$  isotope enriched, and for the  $^{116}\text{Cd}_2\text{Re}_2^{18}\text{O}_7$  at RT.

phase is suppressed by quantum fluctuations, whereas  $^{18}\text{O}$  substitution induces ferroelectric phases with  $T_c$ 's up to  $\sim 25$  K [39–43]. Soft-mode behavior of the vibrational properties has indeed been suggested by preceding Raman spectroscopy measurements which proposed a Goldstone mode at low frequencies [21]. We remark that as the temperature is raised from 5 K to near 80 K, which is well below the SPT from phase II to phase III at 120 K, that the intensity of the mode investigated by Kendziora *et al.* grows towards a maximum.

Summarizing, we have presented remarkable agreement between the *ab initio* calculations of phonon dispersions and the experimental observations which indicates the existence of a novel orthorhombic non-centrosymmetric phase IV in  $\text{Cd}_2\text{Re}_2\text{O}_7$  at  $T < 80$  K. We believe that our findings will shed new light on the understanding of the peculiar metallic properties and the occurrence of the superconducting phase in  $\text{Cd}_2\text{Re}_2\text{O}_7$ .

*Acknowledgments.*— The authors are grateful to Krzysztof Parlinski for the very insightful discussions and comments. This work was supported by the National Science Centre (NCN, Poland) under grants 2017/24/C/ST3/00276 (K.J.K.), 2017/25/B/ST3/02586 (P.P.), and 2016/23/B/ST3/00839 (A.M.O.) and the Natural Sciences and Engineering Research Council (NSERC) of Canada grants DDG-2017-00043 (M.R.) and RGPIN-2018-04438 (F.S.R.). A. M. Oleś is grateful for the Alexander von Humboldt Foundation Fellowship (Humboldt-Forschungspreis).

#### APPENDIX: Low-Temperature Phase: *Ab initio* Phonon Calculations and Raman Scattering

In Section I of this Supplemental Material, we present some additional information on the structural and on the superconducting phase transitions in  $^{116}\text{Cd}_2\text{Re}_2^{18}\text{O}_7$  obtained from experiment. In Section II we present the structural data of  $\text{Cd}_2\text{Re}_2\text{O}_7$  superconductor as obtained from experiment [1] and from the density functional theory calculations.

#### A. Experimental details

In this Section we present detailed results of the characterization of the isotope substituted crystals,  $^{116}\text{Cd}_2\text{Re}_2^{18}\text{O}_7$ , used in the Raman investigation with emphasis on the structural phase transitions (SPTs). Figure 6 displays the heat capacity measured on a crystal of  $^{116}\text{Cd}_2\text{Re}_2^{18}\text{O}_7$ . The well defined  $\lambda$ -type anomaly at the SPT from phase I to phase II is seen at  $\sim 204$  K and a very faint anomaly at  $\sim 114$  K indicating the SPT from phase II to III is revealed, in good agreement with earlier reports [10].

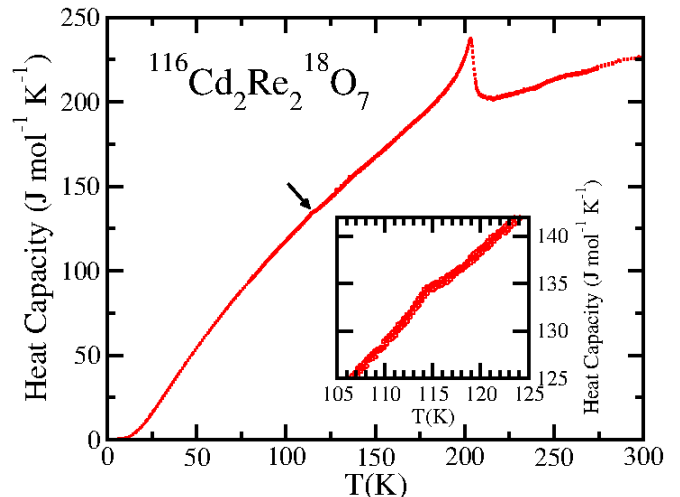


FIG. 6. Specific heat capacity of a crystal of the isotope enriched material,  $^{116}\text{Cd}_2\text{Re}_2^{18}\text{O}_7$ . Anomalies at  $\sim 204$  K and at  $\sim 114$  K (arrow and inset) prove the SPT from phase I to phase II and from phase II to phase III, respectively.

The heat capacity measurements also revealed the anomaly at the  $T_c \sim 1$  K shown in Fig. 7.

Figure 8 shows the splitting of the  $E$  mode observed near  $210\text{ cm}^{-1}$  below  $\sim 80$  K. The red (lower) and green (upper) solid line represents the results of a fit of the center frequencies with a critical power,  $t^\beta$ , where  $t = (T_c - T)/T_c$  and  $\beta = 0.33$  is the critical exponent.  $T_c$  was obtained as  $\sim 81$  K from a fit of the lower branch and kept identical for the upper branch.

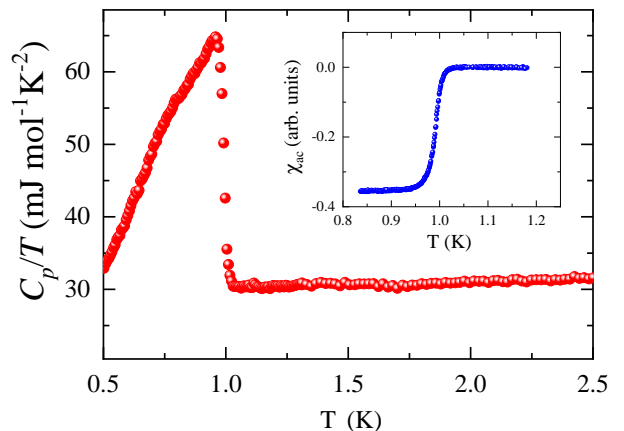


FIG. 7. Specific heat capacity,  $C_p/T$ , of a crystal of the isotope enriched material,  $^{116}\text{Cd}_2\text{Re}_2^{18}\text{O}_7$ , at low temperature. A characteristic  $\lambda$ -type anomaly at the onset of the superconducting phase at  $T_c \sim 1$  K is observed. The inset shows the ac-susceptibility with a distinct drop at  $T_c$ .

TABLE I. Lattice parameters, atomic positions, and total energies in the crystal structures of  $\text{Cd}_2\text{Re}_2\text{O}_7$ .

	Experimental data [44]			DFT calculations		
Phase-I: $Fd\bar{3}m$ (227)						
	$a = b = c = 10.2261(5) \text{ \AA}$			$a = b = c = 10.3816 \text{ \AA}$ $V_I = 1118.90 \text{ \AA}^3, E_I = 0$		
Re	0.2500	0.7500	0.5000	0.0000	0.2500	0.2500
Cd	0.5000	0.5000	0.5000	0.5000	0.5000	0.5000
O(1)	0.3152(9)	0.6250	0.6250	0.3141	0.1250	0.1250
O(2)	0.6250	0.6250	0.6250	0.6250	0.6250	0.6250
Phase-II: $I4m2$ (119)						
	$a = b = 7.2312(3) \text{ \AA}, c = 10.2257(4) \text{ \AA}$			$a = b = 7.3420 \text{ \AA}, c = 10.4101 \text{ \AA}$ $a' = b' = 10.38313 \text{ \AA} (a' = \sqrt{2}a), c' = 10.41010 \text{ \AA}$ $V'_{II} = 1122.31 \text{ \AA}^3, E_{II} = -2.08510 \text{ eV}$		
Re	0.2471(2)	0.0000	0.87294(15)	0.2510	0.0000	0.8760
Cd	0.0000	0.2471(5)	0.6259(3)	0.0000	0.2372	0.6386
O(1)	0.3059(15)	0.1941(15)	0.7500	0.3000	0.2000	0.7500
O(2)	0.0000	0.0000	0.8026(16)	0.0000	0.0000	0.7947
O(3)	0.1889(16)	0.1889(16)	0.0000	0.1795	0.1795	0.0000
O(4)	0.5000	0.0000	0.9317(19)	0.5000	0.0000	0.9189
O(5)	0.0000	0.0000	0.5000	0.0000	0.0000	0.5000
O(6)	0.0000	0.5000	0.7500	0.0000	0.5000	0.7500
Phase-III: $I4_122$ (98)						
	$a = b = 7.2313(3) \text{ \AA}, c = 10.2282(6) \text{ \AA}$			$a = b = 7.3537 \text{ \AA}, c = 10.3729 \text{ \AA}$ $a' = b' = 10.3997 \text{ \AA} (a' = \sqrt{2}a), c' = 10.3729 \text{ \AA}$ $V'_{III} = 1121.87 \text{ \AA}^3, E_{III} = -2.02515 \text{ eV}$		
Re	0.2500	0.9967(3)	0.8750	0.2500	0.0020	0.8750
Cd	0.5041(6)	0.2500	0.1250	0.5229	0.2500	0.1250
O(1)	0.1880(20)	0.1880(20)	0.0000	0.1711	0.1711	0.0000
O(2)	0.5000	0.0000	0.9396(14)	0.5000	0.0000	0.9424
O(3)	0.1970(20)	0.8030(20)	0.0000	0.2032	0.7968	0.0000
O(4)	0.5000	0.5000	0.0000	0.5000	0.5000	0.0000
Phase-IV: $F222$ (22)						
				$a = 10.3832 \text{ \AA}, b = 10.3828 \text{ \AA}, c = 10.4101 \text{ \AA}$ $V_{IV} = 1122.28 \text{ \AA}^3, E_{IV} = -2.08515 \text{ eV}$		
Re				0.124500	0.124502	0.1260
Cd				0.63141	0.63137	0.6114
O(1)				0.5000	0.5000	0.1689
O(2)				0.0706	0.2500	0.2500
O(3)				0.2500	0.4295	0.2500
O(4)				0.5000	0.2000	0.5000
O(5)				0.2000	0.5000	0.5000
O(6)				0.2500	0.2500	0.0447
O(7)				0.5000	0.5000	0.5000
O(8)				0.7500	0.7500	0.7500

## B. Structural data

In Table I we present the structural data as obtained from experiment [44] and from the present density functional theory (DFT) calculations:  $a$ ,  $b$ , and  $c$  denote the lattice parameters, while  $a'$ ,  $b'$ , and  $c'$  denote the sizes of the supercell used for the calculations. Here  $V$  ( $V'$ ) is the volume of the unit cell (supercell). We have included also the total energies given per one supercell with 88 atoms for all studied phases.

\* e-mail: konrad.kapcia@ifj.edu.pl

- [1] M. Smidman, M. B. Salamon, H. Q. Yuan, and D. F. Agterberg, Rep. Prog. Phys. **80**, 036501 (2017).
- [2] Y. Okuda, Y. Miyauchi, Y. Ida, Y. Takeda, C. Tonohiro, Y. Oduchi, T. Yamada, N. D. Dung, T. D. Matsuda, Y. Haga, T. Takeuchi, M. Hagiwara, K. Kindo, H. Harima, K. Sugiyama, R. Settai, and Y. Onuki, J. Phys. Soc. Jpn. **76**, 044708 (2007).
- [3] Y. Yanase and M. Sigrist, J. Phys. Soc. Jpn. **76**, 124709 (2007); **77**, 124711 (2008).

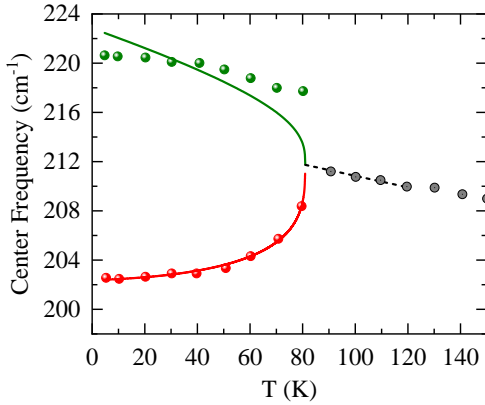


FIG. 8. Splitting of the  $E$  mode observed near  $210 \text{ cm}^{-1}$  versus temperature for  $^{116}\text{Cd}_2\text{Re}_2^{18}\text{O}_7$ . The solid lines represent fits of the center frequencies with a critical power law (see text) indicating a transition temperature of  $\sim 81 \text{ K}$ .

- [4] Y. Matsubayashi, K. Sugii, H. T. Hirose, D. Hirai, S. Sugiyama, T. Terashima, S. Uji, and Z. Hiroi, *J. Phys. Soc. Jpn.* **87**, 053702 (2018).
- [5] W. Witczak-Krempa, G. Chen, Y. B. Kim, and L. Balents, *Annu. Rev. Condens. Matter Phys.*, **5**, 57 (2014).
- [6] R. Schaffer, E. Kin-Ho Lee, B.-J. Yang, and Y. B. Kim, *Rep. Prog. Phys.* **79**, 094504 (2016).
- [7] M. Hanawa, Y. Muraoka, T. Tayama, T. Sakakibara, J. Yamaura, and Z. Hiroi, *Phys. Rev. Lett.* **87**, 187001 (2001).
- [8] H. Sakai, K. Yoshimura, H. Ohno, H. Kato, S. Kambe, R. E. Walstedt, T. D. Matsuda, Y. Haga, and Y. Onuki, *J. Phys.: Condens. Matter* **13**, L785 (2001).
- [9] R. Jin, J. He, S. McCall, C. S. Alexander, F. Drymiotis, and D. Mandrus, *Phys. Rev. B* **64**, 180503(R) (2001).
- [10] Z. Hiroi, J.-I. Yamaura, T. C. Kobayashi, Y. Matsubayashi, and D. Hirai, *J. Phys. Soc. Jpn.* **87**, 024702 (2018).
- [11] J.-I. Yamaura and Z. Hiroi, *J. Phys. Soc. Jpn.* **71**, 2598 (2002).
- [12] Z. Hiroi, J.-I. Yamaura, Y. Muraoka, and M. Hanawa, *J. Phys. Soc. Jpn.* **71**, 1634 (2002).
- [13] I. A. Sergienko and S. H. Curnoe, *J. Phys. Soc. Jpn.* **72**, 1607 (2003).
- [14] I. A. Sergienko, V. Keppens, M. McGuire, R. Jin, J. He, S. H. Curnoe, B. C. Sales, P. Blaha, D. J. Singh, K. Schwarz, and D. Mandrus, *Phys. Rev. Lett.* **92**, 065501 (2004).
- [15] Z. Hiroi and M. Hanawa, *J. Phys. Chem. Solids* **63**, 1021 (2002).
- [16] M. Tachibana, N. Taira, H. Kawaji, and E. Takayama-Muromachi, *Phys. Rev. B* **82**, 054108 (2010).
- [17] H. Harima, *J. Phys. Chem. Solids*, **63**, 1035 (2002).
- [18] D. J. Singh, P. Blaha, K. Schwarz, and J. O. Sofo, *Phys. Rev. B* **65**, 155109 (2002).
- [19] S.-W. Huang, H.-T. Jeng, J.-Y. Lin, W. J. Chang, J. M. Chen, G. H. Lee, H. Berger, H. D. Yang, and K. S. Liang, *J. Phys.: Condens. Matter* **21**, 195602 (2009).
- [20] O. Vyaselev, K. Arai, K. Kobayashi, J. Yamazaki, K. Kodama, M. Takigawa, M. Hanawa, and Z. Hiroi, *Phys. Rev. Lett.* **89**, 017001 (2002).
- [21] C. A. Kendziora, I. A. Sergienko, R. Jin, J. He, V. Keppens, B. C. Sales, and D. Mandrus, *Phys. Rev. Lett.* **95**, 125503 (2005).
- [22] C. S. Knee, J. Holmlund, J. Andreasson, M. Käll, S. G. Eriksson, and L. Börjesson, *Phys. Rev. B* **71**, 214518 (2005).
- [23] J. S. Bae, H. K. Ko, I.-S. Yang, Y. S. Lee, T. W. Noh, R. Jin, J. He, and D. Mandrus, *J. Korean Phys. Soc.* **48**, 946 (2006).
- [24] F. S. Razavi, M. Hajialamdari, M. Reedyk, and R. K. Kremer, *Physica C: Superconductivity and its Applications* **549**, 11 (2018).
- [25] Y. Matsubayashi, T. Hasegawa, N. Ogita, J.-I. Yamaura, and Z. Hiroi, *Physica B* **536**, 600 (2018).
- [26] J. W. Harter, D. M. Kennes, H. Chu, A. de la Torre, Z. Y. Zhao, J.-Q. Yan, D. G. Mandrus, A. J. Millis, and D. Hsieh, *Phys. Rev. Lett.* **120**, 047601 (2018).
- [27] J. W. Harter, Z. Y. Zhao, J.-Q. Yan, D. G. Mandrus, and D. Hsieh, *Science* **356**, 295 (2017).
- [28] N. L. Wang, J. J. McGuire, T. Timusk, R. Jin, J. He, and D. Mandrus, *Phys. Rev. B* **66**, 014534 (2002).
- [29] M. Hajialamdari, F. S. Razavi, D. A. Crandles, R. K. Kremer, and M. Reedyk, *J. Phys.: Condens. Matter* **2**, 505701 (2012).
- [30] M. Hajialamdari, F. S. Razavi, and M. Reedyk, *Physica B* **502**, 170 (2016).
- [31] F. S. Razavi, Y. Rohanizadegan, M. Hajialamdari, M. Reedyk, R. K. Kremer, and B. Mitrović, *Can. J. Phys.* **93**, 1 (2015).
- [32] P. E. Blöchl, *Phys. Rev. B* **50**, 17953 (1994).
- [33] G. Kresse and D. Joubert, *Phys. Rev. B* **59**, 1758 (1999).
- [34] J. P. Perdew, K. Burke, and M. Ernzerhof, *Phys. Rev. Lett.* **77**, 3865 (1996); *Phys. Rev. Lett.* **78**, 1396 (1997).
- [35] G. Kresse and J. Furthmüller, *Phys. Rev. B* **54**, 11169 (1996); *Comput. Mater. Sci.* **6**, 15 (1996).
- [36] K. Parlinski, Z. Q. Li, and Y. Kawazoe, *Phys. Rev. Lett.* **78**, 4063 (1997).
- [37] K. Parlinski, Software PHONON ver. 6.15, Cracow, Poland (2015).
- [38] K. Lejaeghere, *et al.*, *Science* **351**, aad3000-1 (2016).
- [39] M. Itoh, R. Wang, Y. Inaguma, T. Yamaguchi, Y.-J. Shan, and T. Nakamura, *Phys. Rev. Lett.* **82**, 3540 (1999).
- [40] A. Bussmann-Holder, H. Büttner, and A. R. Bishop, *J. Phys.: Condens. Matter* **12**, L115 (2000); *Phys. Rev. Lett.* **99**, 167603 (2007).
- [41] Y. Yamada, N. Todoroki, and S. Miyashita, *Phys. Rev. B* **69**, 024103 (2004).
- [42] S. E. Rowley, L. J. Spalek, R. P. Smith, M. P. M. Dean, M. Itoh, J. F. Scott, G. G. Lonzarich, and S. S. Saxena, *Nature Phys.* **10**, 367 (2014).
- [43] J. M. Edge, Y. Kedem, U. Aschauer, N. A. Spaldin, and A. V. Balatsky, *Phys. Rev. Lett.* **115**, 247002 (2015).
- [44] S.-W. Huang, H.-T. Jeng, J.-Y. Lin, W. J. Chang, J. M. Chen, G. H. Lee, H. Berger, H. D. Yang, and K. S. Liang, *J. Phys.: Condens. Matter* **21**, 195602 (2009).